

Periodic and chaotic oscillations in mutual-coupled mid-infrared quantum cascade lasers

Zhi-Wei Jia(贾志伟), Li Li(李丽), Yi-Yan Guo(郭一岩), An-Bang Wang(王安帮), Hong Han(韩红), Jin-Chuan Zhang(张锦川), Pu Li(李璞), Shen-Qiang Zhai(翟慎强), and Feng-Qi Liu(刘峰奇)

Citation: Chin. Phys. B, 2022, 31 (**10**): 100505. DOI: 10.1088/1674-1056/ac8f34
Journal homepage: http://cpb.iphy.ac.cn; http://iopscience.iop.org/cpb

What follows is a list of articles you may be interested in

Cascade discrete memristive maps for enhancing chaos

Fang Yuan(袁方), Cheng-Jun Bai(柏承君), and Yu-Xia Li(李玉霞)
Chin. Phys. B, 2021, 30 (**12**): 120514. DOI: 10.1088/1674-1056/ac20c7

Controlling chaos and supressing chimeras in a fractional-order discrete phase-locked loop using impulse control

Karthikeyan Rajagopal, Anitha Karthikeyan, and Balamurali Ramakrishnan
Chin. Phys. B, 2021, 30 (**12**): 120512. DOI: 10.1088/1674-1056/ac1b83

Nonlinear dynamics in non-volatile locally-active memristor for periodic and chaotic oscillations

Wen-Yu Gu(谷文玉), Guang-Yi Wang(王光义), Yu-Jiao Dong(董玉姣), and Jia-Jie Ying(应佳捷)
Chin. Phys. B, 2020, 29 (**11**): 110503. DOI: 10.1088/1674-1056/ab9ded

A flux-controlled model of meminductor and its application in chaotic oscillator

Guang-Yi Wang(王光义), Pei-Pei Jin(靳培培), Xiao-Wei Wang(王晓炜), Yi-Ran Shen(沈怡然), Fang Yuan(袁方), Xiao-Yuan Wang(王晓媛)
Chin. Phys. B, 2016, 25 (**9**): 090502. DOI: 10.1088/1674-1056/25/9/090502

Hysteresis-induced bifurcation and chaos in a magneto-rheological suspension system under external excitation

Hailong Zhang(张海龙), Enrong Wang(王恩荣), Fuhong Min(闵富红), Ning Zhang(张宁)
Chin. Phys. B, 2016, 25 (**3**): 030503. DOI: 10.1088/1674-1056/25/3/030503

Periodic and chaotic oscillations in mutual-coupled mid-infrared quantum cascade lasers

Zhi-Wei Jia(贾志伟)[1,2], Li Li(李丽)[1], Yi-Yan Guo(郭一岩)[1], An-Bang Wang(王安帮)[1,†], Hong Han(韩红)[1], Jin-Chuan Zhang(张锦川)[2], Pu Li(李璞)[1], Shen-Qiang Zhai(翟慎强)[2], and Feng-Qi Liu(刘峰奇)[2]

[1] *Key Laboratory of Advanced Transducers and Intelligent Control System, Ministry of Education and Shanxi Province, College of Physics and Optoelectronics, Taiyuan University of Technology, Taiyuan* 030024, *China*

[2] *Key Laboratory of Semiconductor Materials Science, Beijing Key Laboratory of Low Dimensional Semiconductor Materials and Devices, Institute of Semiconductors, Chinese Academy of Sciences, Beijing* 100083, *China*

(Received 21 April 2022; revised manuscript received 9 August 2022; accepted manuscript online 5 September 2022)

Dynamic states in mutual-coupled mid-infrared quantum cascade lasers (QCLs) were numerically investigated in the parameter space of injection strength and detuning frequency based on the Lang–Kobayashi equations model. Three types of period-one states were found, with different periods of injection time delay τ_{inj}, $2\tau_{inj}$, and reciprocal of the detuning frequency. Besides, square-wave, quasi-period, pulse-burst and chaotic oscillations were also observed. It is concluded that external-cavity periodic dynamics and optical modes beating are the mainly periodic dynamics. The interaction of the two periodic dynamics and the high-frequency dynamics stimulated by strong injection induces the dynamic states evolution. This work helps to understand the dynamic behaviors in QCLs and shows a new way to mid-infrared wide-band chaotic laser.

Keywords: periodic oscillations, chaotic oscillations, mutual-coupled quantum cascade lasers

PACS: 05.45.–a, 05.45.Pq, 42.55.Px **DOI:** 10.1088/1674-1056/ac8f34

1. Introduction

Quantum cascade lasers (QCLs) are very promising mid-infrared semiconductor lasers, which have been proven to be powerful and versatile.[1,2] By elaborately designing the structure of the active zone superlattice, the wavelength of QCLs can be tailored to cover the whole mid-infrared region.[3–5] Because of the lower transmission loss and higher scattering tolerance in the mid-infrared atmospheric windows bands (3 μm–5 μm and 8 μm–14 μm) compared to the well-developed near-infrared bands, QCLs can find applications in diverse fields, such as free space communications,[6–8] laser ranging,[9] remote sensing,[10,11] and optoelectronic countermeasure.[12]

In the practical use, the stability of QCLs subject to inevitable external optical perturbation is very important, while the dynamic behaviors of QCLs have not been well understood. External optical perturbation can drive near-infrared semiconductor lasers, which are based on inter-band transition, from stable state to various dynamic states, including periodic oscillation,[13,14] chaotic laser state,[15,16] low-frequency fluctuations,[17–19] regular pulse packages,[20] etc. Unlike inter-band semiconductor lasers, QCLs are based on the inter-subband electron transition,[1] with ultrafast carrier dynamics[21] and theoretically near-zero linewidth enhancement factor (α-factor).[22] As a result, QCLs seem to be more stable to external optical perturbation.[23] However, dynamic states of QCLs are often observed in applications and researches. In 2016, Grillot *et al*. reported the experimental observation of low-frequency chaotic laser in a distributed feedback (DFB) QCL with external optical feedback.[24] Recently, Wang *et al*. observed low-frequency oscillations in QCLs with tilted optical feedback.[25,26] There are also some theoretical models, based on rate equations or Maxwell–Bloch equations, demonstrating periodic oscillations,[27] self-pulsations,[28] low-frequency fluctuations,[24] even wide-band chaotic laser in QCLs.[29] But these works are not enough to understand the dynamic behaviors of QCLs. Experimental observation of high-frequency dynamic oscillations is still lacking, apart from the active modulation and self-pulsations. The wide-band chaotic laser predicted by Ref. [29] cannot be observed even the feedback strength is higher than 60% in our experiment.

The high-frequency periodic oscillation in inter-band semiconductor lasers is always related to the relaxation oscillation dynamic, and the wide-band chaotic laser state is usually resulted from the interaction of the external periodic dynamic and the relaxation oscillation dynamic. But the relaxation oscillation is absent in QCLs because of the ultrafast carrier dynamics.[30] We can deduce that the high-frequency oscillation in QCLs should be related to a high-frequency dynamic, such as optical modes beating.

In this work, we numerically investigated the dynamic states in mutual-coupled mid-infrared QCLs based on the Lang–Kobayashi equations. The two QCLs had different optical frequencies to bring in optical modes beating dynamic. The external-cavity length between the two QCLs was $L =$

†Corresponding author. E-mail: wanganbang@tyut.edu.cn

© 2022 Chinese Physical Society and IOP Publishing Ltd

1.5 m, corresponding to the injection time delay $\tau_{inj} = L/c$. When the injection strength k_{inj} was as low as 0.1, three types of period-one states with different periods were found, which were injection time delay τ_{inj}, $2\tau_{inj}$, and reciprocal of the detuning frequency. The evolution of dynamic states at different frequency detuning Δf was also studied as k_{inj} increased. Several dynamic states were observed, including period-one, square-wave, quasi-period, pulse-burst and chaos. The physics mechanism of the dynamical evolution was discussed. It can be concluded that: (i) external-cavity dynamic and optical modes beating are the mainly periodic dynamics; (ii) strong injection can stimulate strong optical nonlinear and high-order harmonics dynamics to break the periodic oscillations; (iii) the complex pulse-burst and chaotic states are resulted from the interaction of the external-cavity periodic dynamic and optical modes beating and the stimulation of optical nonlinear.

2. Theoretical model

Figure 1 shows the schematic of the two-stage band structure of a typical mid-infrared QCLs active zone and the structure diagram of the mutual-coupled QCLs. As shown in Fig. 1(a), each stage of the QCLs active zone is composed of an extraction/injection region and an active region. Electrons from the last stage are injected into the energy level 3 of the active region by the extraction/injection region. Then electrons in the energy level 3 transit to the energy level 2 with the time τ_{32}, meanwhile, photons are stimulated. Subsequently, electrons in the energy level 2 are scattered to the energy level 1 by longitudinal-optical phonons with the time τ_{21}. Afterwards electrons in the energy level 1 are extracted and injected into the next stage with the time τ_{out}. Because τ_{21} and τ_{out} are shorter than τ_{32}, population inversion occurs between the energy level 3 and the energy level 2. Though electrons in the energy level 3 also transit to the energy level 1 with the time τ_{31}, population inversion does not occur between the energy level 3 and the energy level 1 because of the very short τ_{21}. Based on the band structure, the rate equations describing the number of carriers are as follows:

$$\frac{dN_{3_1,2}(t)}{dt} = \eta\frac{I_{1,2}}{q} - \frac{N_{3_1,2}(t)}{\tau_{32}} - \frac{N_{3_1,2}(t)}{\tau_{31}} - G_0\Delta N_{1,2}S_{1,2}(t), \quad (1)$$

$$\frac{dN_{2_1,2}(t)}{dt} = \frac{N_{3_1,2}(t)}{\tau_{32}} - \frac{N_{2_1,2}(t)}{\tau_{21}} + G_0\Delta N_{1,2}S_{1,2}(t), \quad (2)$$

$$\frac{dN_{1_1,2}(t)}{dt} = \frac{N_{3_1,2}(t)}{\tau_{31}} + \frac{N_{2_1,2}(t)}{\tau_{21}} - \frac{N_{1_1,2}(t)}{\tau_{out}}, \quad (3)$$

where N_3, N_2, and N_1 represent the numbers of carriers in the energy level 3, the energy level 2, and the energy level 1, $\Delta N_{1,2} = N_{3_1,2} - N_{2_1,2}$, η is the current injection efficiency, I is the pump current, q is the elementary charge, G_0 is the gain coefficient. S represents the number of photons. The subscripts 1,2 correspond to QCL_1 and QCL_2, respectively.

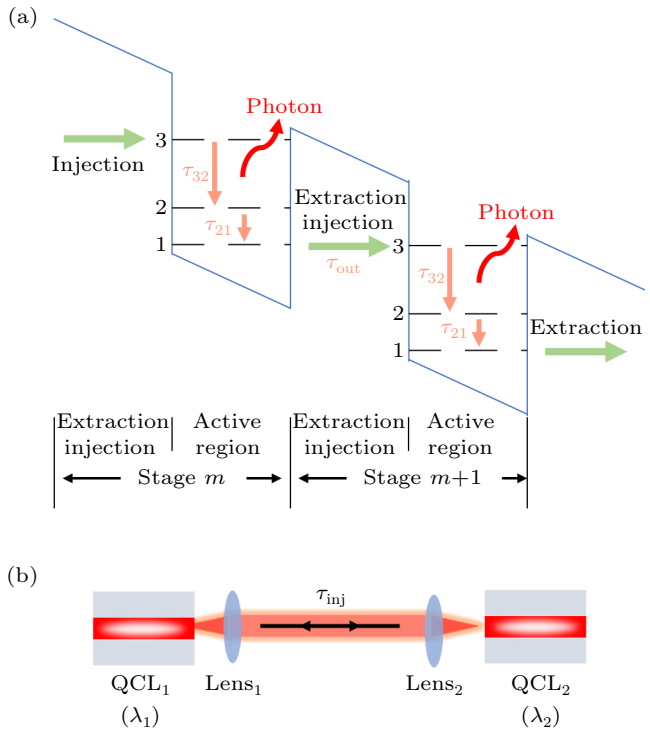


Fig. 1. (a) Schematic of two-stage band structure of QCLs active zone. (b) Structure diagram of mutual-coupled QCLs.

As shown in Fig. 1(b), the laser emitted from $QCL_{1,2}$ is collimated by $lens_{1,2}$, then is focused and injected into $QCL_{2,1}$ by $lens_{2,1}$. The injection time delay τ_{inj} is fixed at 5 ns. Based on the mutual-coupled structure and Lang–Kobayashi equation, the rate equations describing the number of photons and phase in the mutual-coupled QCLs are as follows:

$$\frac{dS_{1,2}(t)}{dt} = \left(mG_0\Delta N_{1,2} - \frac{1}{\tau_p}\right)S_{1,2}(t) + m\beta\frac{N_{3_1,2}(t)}{\tau_{sp}} + 2\frac{\sqrt{k_{inj_21,12}}}{\tau_L}\sqrt{S_{2,1}(t-\tau_{inj})S_{1,2}(t)}\cos\theta_{1,2}(t), \quad (4)$$

$$\frac{d\varphi_{1,2}(t)}{dt} = \frac{1}{2}\alpha\left(mG_0\Delta N_{1,2} - \frac{1}{\tau_p}\right) - \frac{\sqrt{k_{inj_21,12}}}{\tau_L}\sqrt{\frac{S_{2,1}(t-\tau_{inj})}{S_{1,2}(t)}}\sin\theta_{1,2}(t), \quad (5)$$

where φ represents the phase of the optical field, m is the stage number in the active zone, β is the spontaneous emission factor, τ_{sp} is the spontaneous emission time, k_{inj} is the injection strength, which is defined by the ratio of the injected laser power and the intrinsic laser power, τ_L is the round-trip time inside the laser cavity, α is the linewidth enhancement factor of QCLs, which is smaller than that in traditional inter-band semiconductor lasers. The coupling phase $\theta_{1,2}$ is

$$\theta_{1,2}(t) = \omega_{2,1}\tau_{inj} \mp \Delta\omega t - \varphi_{2,1}(t-\tau_{inj}) + \varphi_{1,2}(t), \quad (6)$$

where $\omega_{2,1} = 2\pi c/\lambda_{2,1}$ is the angular frequency of $QCL_{2,1}$, $\Delta\omega = |\omega_1 - \omega_2|$ is the angular frequency detuning between

QCL_1 and QCL_2, and frequency detuning $\Delta f = \Delta\omega/2\pi$. It is noted that the internal parameters of the two QCLs are exactly same, except for the central frequency of QCLs. The descriptions of symbols and the selected values for simulation are shown in Table 1, unless stated otherwise.[24,27,29]

Table 1. The used parameters for the simulation.

Symbol	Description	Value
η	current injection efficiency	0.45
I	pump current	$2I_{th}$
I_{th}	threshold current	425 mA
q	elementary charge	1.6×10^{-19} C
τ_{32}	transition time from level 3 to 2	2.0 ps
τ_{31}	transition time from level 3 to 2	2.4 ps
G_0	gain coefficient	5.3×10^{4} s^{-1}
τ_{21}	transition time from level 2 to 1	0.5 ps
τ_{out}	extraction/injection time	0.5 ps
τ_{inj}	injection time delay	5 ns
m	stage number	30
τ_p	photon lifetime	4.7 ps
β	spontaneous emission factor	1×10^{-6}
τ_{sp}	spontaneous emission time	7 ns
τ_L	round-trip time inside cavity	21.3 ps
α	linewidth enhancement factor	1.7
c	velocity of light in vacuum	3×10^{8} m/s
λ	wavelength	4.5 μm

The rate Eqs. (1)–(5) are numerically solved by using the fourth-order Runge–Kutta method with time lag 0.1 ps. The obtained $S(t)$ is regarded as the time series of laser intensity. The electric field of laser can be described by

$$E(t) = \sqrt{S(t)}\cos[\omega t + \varphi(t)], \tag{7}$$

where ω is the angular frequency of QCL. The Fourier transforms of $S(t)$ and $E(t)$ are used to describe the power spectra and optical spectra.

3. Results and discussion

3.1. Absence of the relaxation oscillation

Firstly, we solved the rate equations of free-running QCL and studied the response of the QCL by applying the step current, where the current was increased from low-level current I_{th} to a high-level current. Figure 2(a) shows the QCL responses with the high-level currents of $1.01I_{th}$ and $2I_{th}$. As shown, the photon number monotonically increases from the low-level value to the high-level value. There is no relaxation oscillation occurring, which is similar to the existed viewpoint.[30] The response times, which are defined as the time of photon number increasing from 10% to 90%, are respectively 12.18 ps and 11.31 ps when the high-level currents are $1.01I_{th}$ and $2I_{th}$. Figure 2(b) plots the response time as a function of the high-level current. As the high-level current increases, the response time decreases. This indicates that a high current can enhance fast dynamics in QCLs. Therefore, we chose the high pump current of $2I_{th}$, with the α equal to 1.7, in the following work.

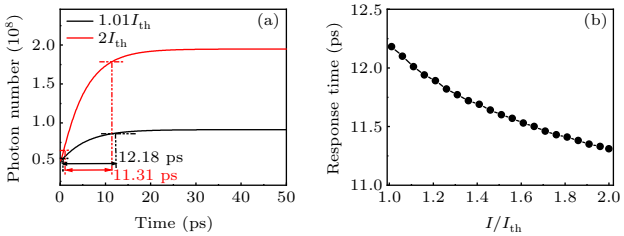


Fig. 2. (a) QCL response with the high-level current of $1.01I_{th}$ and $2I_{th}$. (b) The response time as a function of the high-level current.

3.2. Three types of period-one states

Secondly, we solved the rate equations of the mutual-coupled QCLs with fixed injection strength $k_{inj} = 0.1$ and varying the detuning frequency Δf. The nonlinear dynamic states of the two QCLs are similar, therefore, we only show the results of QCL_1 in this paper.

Three types of period-one (P1) states with different periods are found. The time series, power spectra and optical spectra are plotted in Fig. 3. At $\Delta f = 0$ GHz, as shown in Fig. 3(a), sinusoid-like time series with the period of the injection time delay τ_{inj} is observed, with a fundamental frequency peak of 0.2 GHz and very low harmonic peaks in the power spectrum. In the optical spectrum, there are a cluster of peaks with the interval of 0.2 GHz. This is different from the P1 state of the inter-band semiconductor lasers, where the fundamental frequency is mainly determined by the relaxation oscillation. At $\Delta f = 1$ GHz, as shown in Fig. 3(b), the period is equal to twice the injection time delay ($2\tau_{inj}$), with a fundamental frequency peak of 0.1 GHz in the power spectrum. In the optical spectrum, the interval of peaks is also 0.1 GHz. At $\Delta f = 20$ GHz, as shown in Fig. 3(c), the period is about 51.4 ps, the fundamental frequency peak in the power spectrum is $f_\Delta \sim 19.438$ GHz, and the interval of peaks in the optical spectrum is also f_Δ.

In our model, $\Delta f = 0$ GHz means that QCL_1 and QCL_2 are exactly identical. Therefore, the mutual-coupled structure is equivalent to self-injection with a time delay. The P1 state with the period of τ_{inj} can be identified as the dynamic oscillation from the external-cavity periodic dynamics, which is also observed in the vertical-cavity surface-emitting laser.[32] Actually, there will never be two identical QCLs. The situation at $\Delta f = 0$ GHz will not be described in following. When $\Delta f \neq 0$ GHz and is small, complete injection locking is easily realized in the mutual-coupled QCLs. Complete injection locking means that the intrinsic resonant mode is suppressed. In this case, the laser mode is decided by the injected field, and one QCL is an optical modulation and feedback component for the other QCL. The P1 state with the period of $2\tau_{inj}$ is corresponding to the gradual mode hopping, which is resulted from

the external-cavity optical injection. In Fig. 3(b), two peaks with the interval of $\Delta f = 1$ GHz can also be observed in the optical spectrum, while the peak of 1 GHz cannot be observed in the power spectrum. This indicates that the two modes do not exist simultaneously, which also proves the mode hopping. Due to the existence of a series of external-cavity modes, the time series is sinusoidal-like. When Δf increases to 20 GHz, injection locking is not complete, i.e., the intrinsic resonant mode will not be suppressed by the optical injection. In this case, the intrinsic resonant mode and the laser mode from optical injection coexist in QCLs. As shown in Fig. 3(c3), more than two peaks can be observed, which demonstrates that the relative phase between the two modes is locked by mutual injection. Therefore, the P1 state with the period of f_Δ is induced by optical modes beating. The oscillation frequency f_Δ is slightly smaller than Δf, which is the same as that in QCL with unidirectional optical injection.[27] Because the pulling effect in QCLs dominates over the red-shift effect, the injected mode pulls the resonant mode away from its free-running frequency towards the injected one.

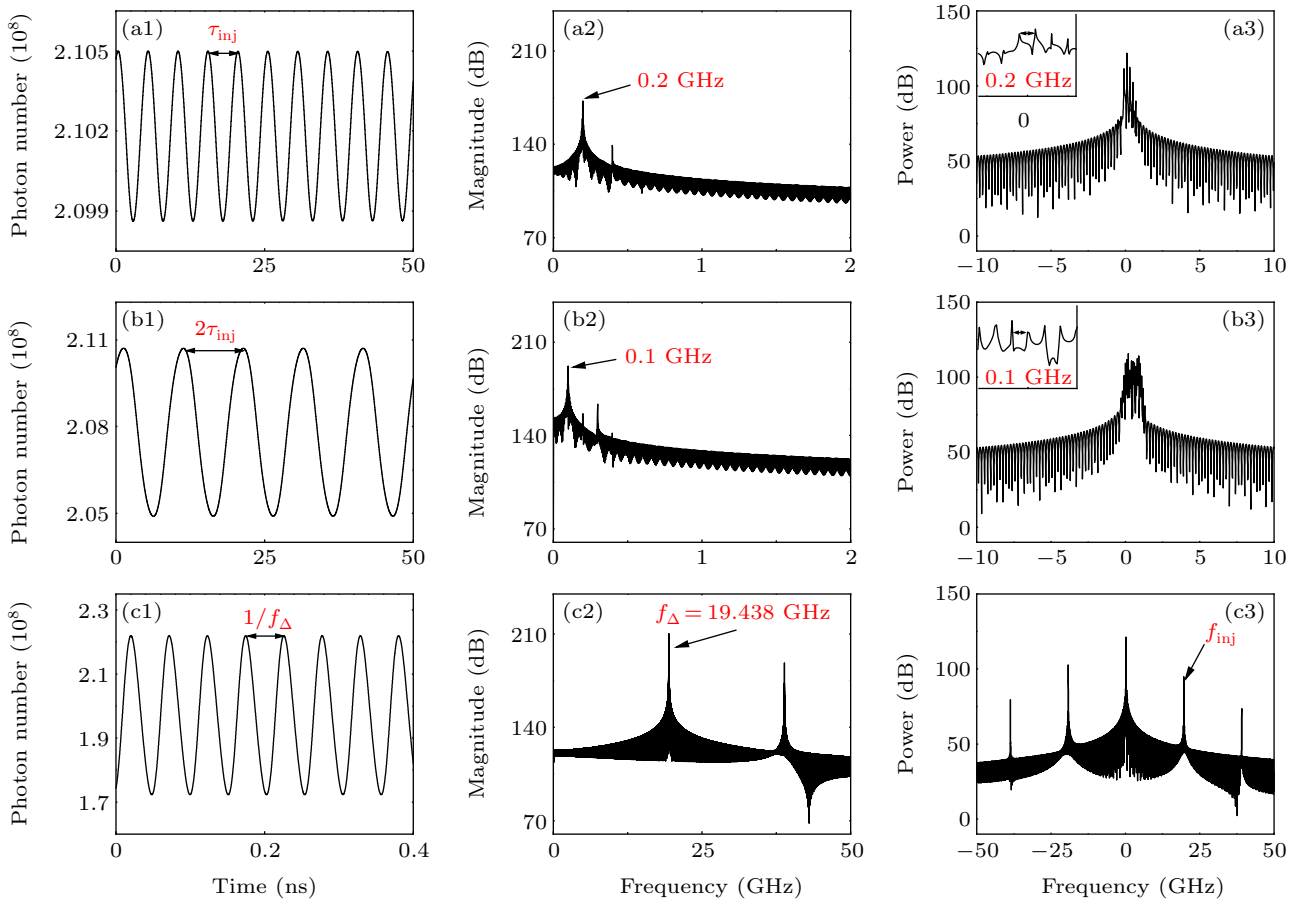


Fig. 3. Three types of period-one states at detuning frequency (a) $\Delta f = 0$ GHz, (b) $\Delta f = 1$ GHz, (c) $\Delta f = 20$ GHz, with fixed injection strength $k_{inj} = 0.1$. Column 1 shows time series, column 2 shows power spectra and column 3 shows optical spectra. The insets in (a3) and (b3) show the enlarged view around the peaks. The f_{inj} is the optical frequency of the laser mode resulted from optical injection.

3.3. Influence of injection strength at different detuning frequencies

Furtherly, we studied the evolution of dynamic states by increasing injection strength k_{inj} at the Δf of 2 GHz, 7 GHz, 14 GHz, 20 GHz, and 29 GHz, which corresponded to the five typical evolution routes.

Figure 4 depicts the time series, power spectra and optical spectra at $\Delta f = 2$ GHz with different k_{inj}. At $k_{inj} = 0.1$, as shown in Fig. 4(a), the P1 state is similar to that in Fig. 3(b). The time series shows a distorted sinusoidal waveform and hence high-order harmonic peaks arise in the power spectra. The distorted waveform is corresponding to the decreased injection locking when Δf increases. At $k_{inj} = 0.45$, as shown in Fig. 4(b), the time series is a square wave (SW) with the period of $2\tau_{inj}$ and duty cycle of about 40%. In the optical spectrum, the external-cavity modes are weakened, the intrinsic resonant mode and the injected laser mode become obvious. It can be explained by that the stronger injection enhances the stability of laser modes, to some extent, suppressing the external-cavity modes. As a result, the time series transfers into SW. At $k_{inj} = 0.58$, QCLs exhibit quasi-periodic (QP) oscillation, with the consistent period with that of Figs. 4(a) and 4(b). And the wavelength blueshift can be observed in the optical spectrum, with more external-cavity modes. This indicates that strong nonlinear optical action occurs and breaks the injection locking, leading to the QP oscillation.

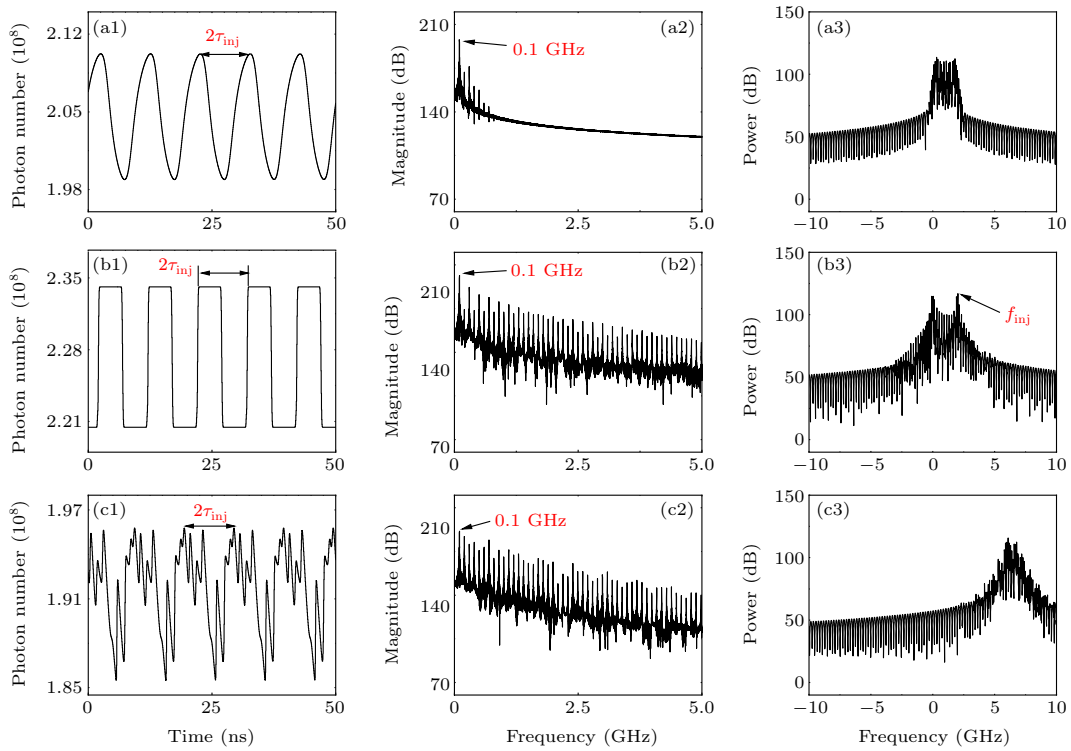


Fig. 4. Time series, power spectra and optical spectra at $\Delta f = 2$ GHz for injection strength k_{inj} of (a) 0.1, (b) 0.45, and (c) 0.58.

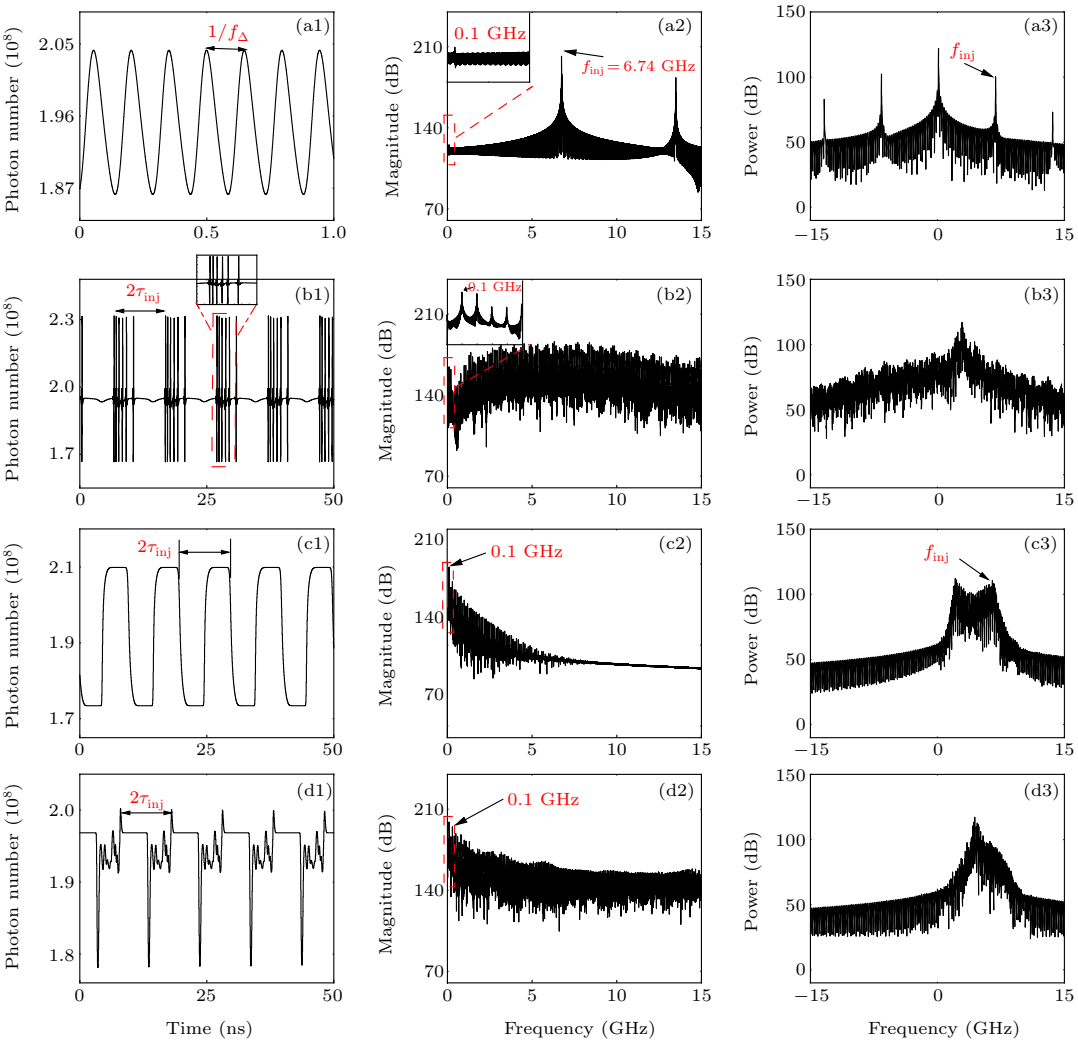


Fig. 5. Time series, power spectra and optical spectra at $\Delta f = 7$ GHz for injection strength k_{inj} of (a) 0.01, (b) 0.13, (c) 0.25, and (d) 0.35.

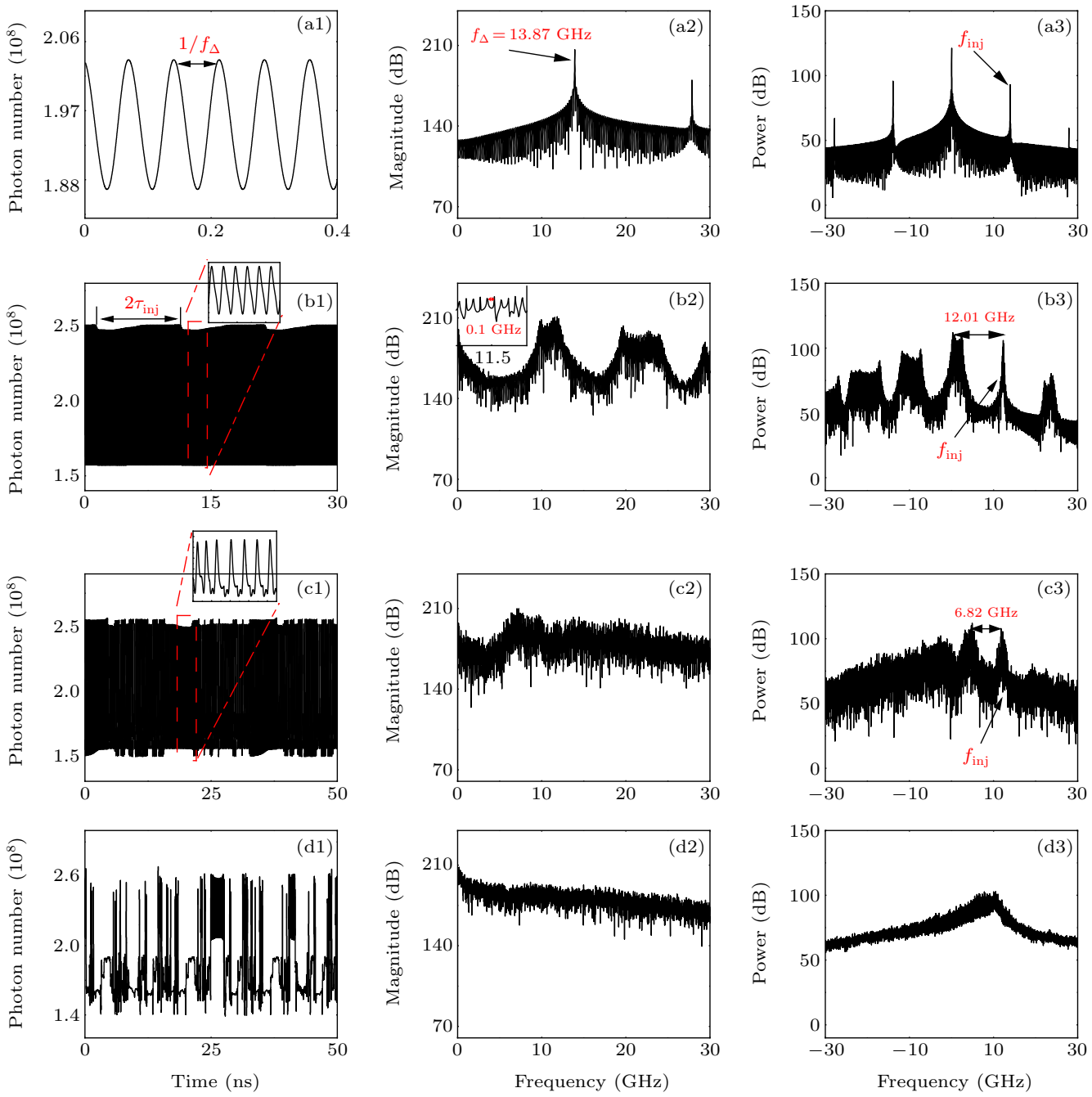


Fig. 6. Time series, power spectra and optical spectra at $\Delta f = 14$ GHz for injection strength k_{inj} of (a) 0.01, (b) 0.3, (c) 0.35, and (d) 0.4. The inset in (b2) shows the enlarged view around the peaks.

Figure 5 shows the time series, power spectra and optical spectra at $\Delta f = 7$ GHz with different k_{inj}. At $k_{inj} = 0.01$, as shown in Fig. 5(a), the P1 state resulted from optical modes beating is observed. The time series has a sinusoidal waveform. There exists a sharp peak at f_Δ of 6.74 GHz and a small peak at external-cavity frequency f_{EC} of 0.1 GHz in the power spectrum. The optical spectrum is similar to that in Fig. 3(c3). At $k_{inj} = 0.13$, the QCLs exhibit pulse burst (PB) state with stable amplitude and a burst period of $2\tau_{inj}$, and the pulses do not have evident periodicity. The power spectrum seems to indicate chaotic state with external-cavity periodic peaks. So the PB state can be thought as an intermittent chaotic state. In the optical spectrum, a wide envelope peak with a sharp central peak can be observed. The envelope peak and sharp peak correspond to the stable parts and the PB parts, respectively. As k_{inj} increases, the number of pulses in one burst decreases. At $k_{inj} = 0.25$, QCLs exhibit SW state with the period of $2\tau_{inj}$ and duty cycle of 30%. At $k_{inj} = 0.35$, QCLs exhibit QP state. The SW and QP states are similar to those at $\Delta f = 2$ GHz.

Figure 6 shows the time series, power spectra and optical spectra at $\Delta f = 14$ GHz with different k_{inj}. At $k_{inj} = 0.01$, as shown in Fig. 6(a), the P1 state resulted from optical modes beating with the sinusoidal time series is observed. There are only sharp peaks at integer multiple f_Δ in the power spec-

trum. The external-cavity periodic dynamic is completely suppressed. The optical spectrum is similar to that in Fig. 3(c3). At $k_{inj} = 0.3$, both the optical modes beating periodic dynamic and the external-cavity periodic dynamic become evident in the time series and power spectrum. Here we choose a critical periodicity suppression ratio of 20 dB. If the optical modes beating peak is 20 dB higher than the external-cavity periodic peak in the power spectrum, the dynamic state can be thought as P1 state. Otherwise, it is QP state, which is different from the QP state in Figs. 4(c) and 5(d). In the optical spectrum, the f_Δ is 12.01 GHz. At $k_{inj} = 0.35$, the QCLs exhibit a weak chaotic state, with evident envelope peaks in the power and optical spectra. The f_Δ is 6.82 GHz. At $k_{inj} = 0.4$, the QCLs exhibit a strong chaotic state, with a wide-band and flat power spectrum and a very wide envelope optical spectrum. In the optical spectrum, only one envelope peak can be observed.

Figure 7 shows the time series, power spectra and optical spectra at $\Delta f = 20$ GHz with different k_{inj}. At $k_{inj} = 0.01$, the QCLs exhibit the similar P1 state to that shown in Fig. 6(a). The external-cavity periodic dynamic is completely suppressed. At $k_{inj} = 0.39$, the QCLs exhibit the similar QP state to that shown in Fig. 6(b). In the optical spectrum, the f_Δ is 16.79 GHz. At $k_{inj} = 0.55$, the QCLs exhibit a chaotic state with a wide-band and flat power spectrum and a very wide envelope optical spectrum. But the chaotic state is different from that in Fig. 6(d). There is a very wide envelope peak around 20 GHz in the power spectrum. In the optical spectrum, there are two envelope peaks with the interval of 20.98 GHz.

We think that the two chaotic states in the mutual-coupled QCLs have different physical origins. When Δf is small, the pulling effect under strong injection can make the intrinsic resonant mode and injected mode very close, leading to strong interaction of the external-cavity periodic dynamic and optical modes beating. As a result, chaotic oscillation occurs. In the optical spectrum, there is only one wide envelope peak. When Δf is large, the pulling effect will be disabled as k_{inj} increases, because of the strong optical nonlinear. Though the interaction of the external-cavity periodic dynamic and optical modes beating is weakened, the strong optical nonlinear can also break the periodic oscillation, leading to the chaotic oscillation. In the optical spectrum, there are two envelope peaks with the interval of Δf.

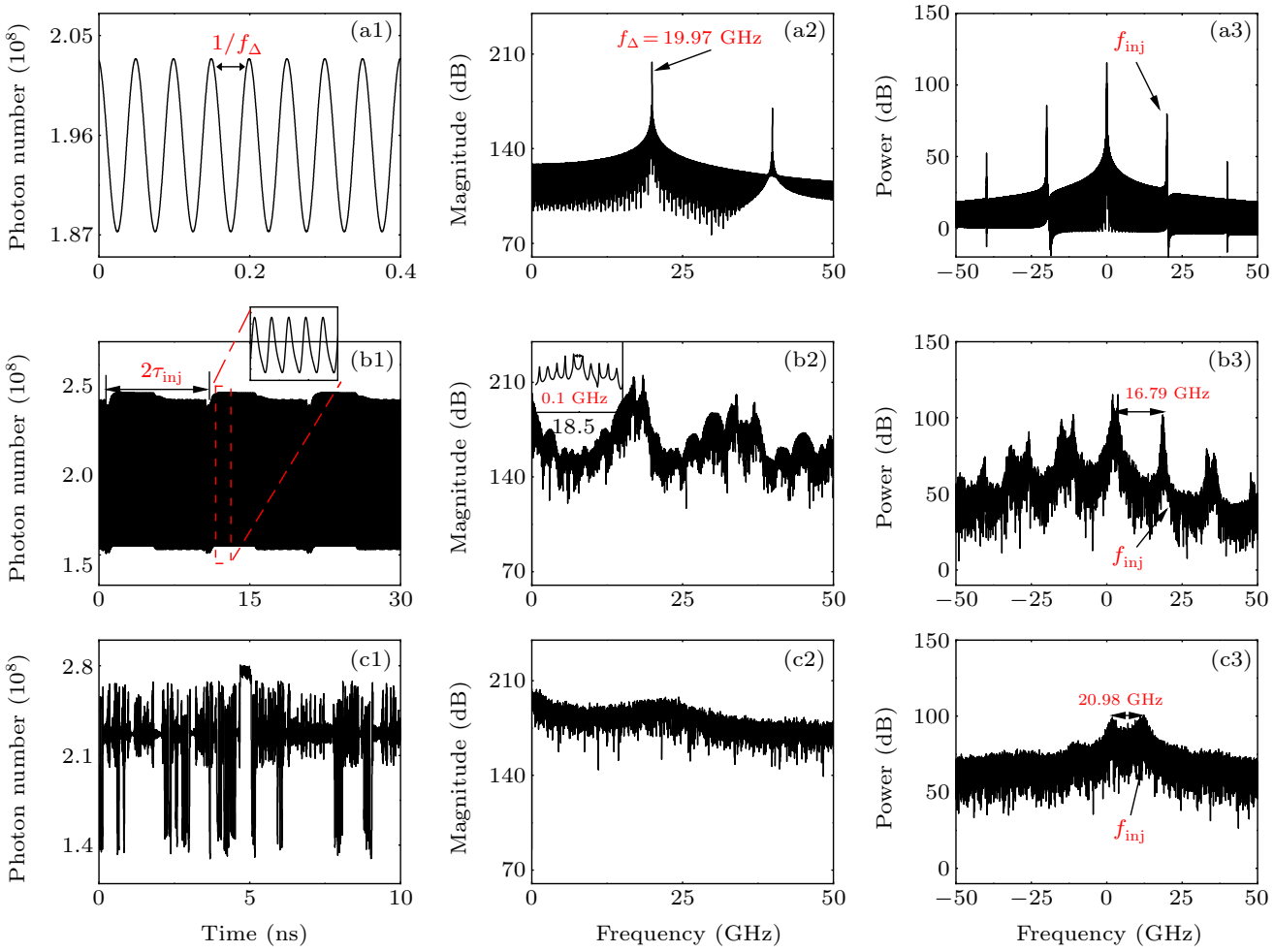


Fig. 7. Time series, power spectra and optical spectrum at $\Delta f = 20$ GHz for injection strength k_{inj} of (a) 0.01, (b) 0.39, and (c) 0.55. The inset in (b2) shows the enlarged view around the peaks.

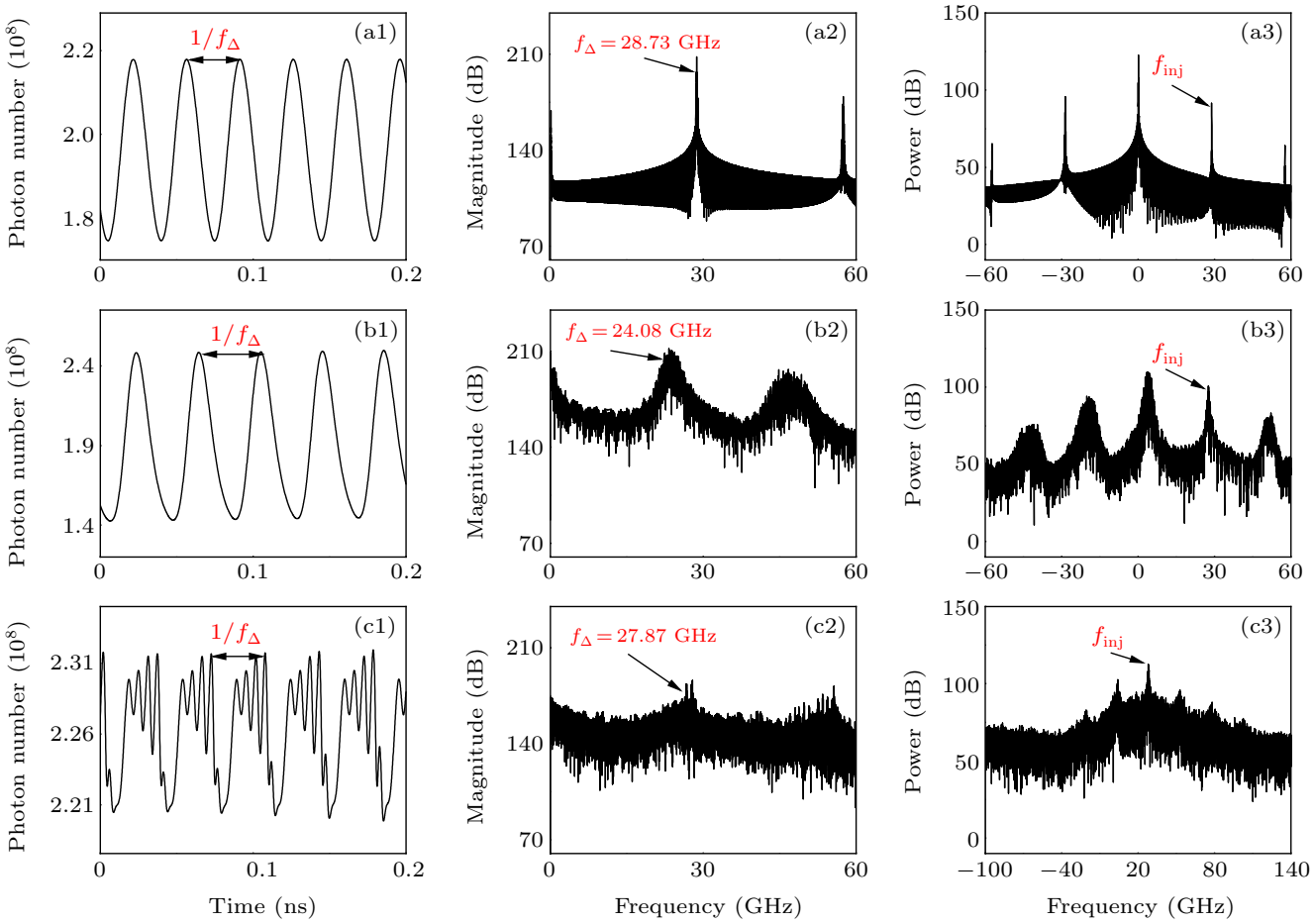


Fig. 8. Time series, power spectra and optical spectrum at $\Delta f = 29$ GHz for injection strength $k_{\rm inj}$ of (a) 0.1, (b) 0.57 and (c) 0.59.

Figure 8 shows the time series, power spectra and optical spectra at $\Delta f = 29$ GHz with different $k_{\rm inj}$. At $k_{\rm inj} = 0.1$, the QCLs exhibit the P1 state resulted from optical modes beating, with very sharp peaks at integer multiple f_Δ in the power spectrum. A small peak at $f_{\rm EC}$ can also be observed. As $k_{\rm inj}$ increases, the peaks at integer multiple f_Δ are gradually broadened and the peaks at integer multiple $f_{\rm EC}$ are gradually heightened. At $k_{\rm inj} = 0.57$, the peak at $f_\Delta = 24.08$ GHz is still 24 dB higher than that at $f_{\rm EC} = 0.1$ GHz. The dynamic state is P1 state. At $k_{\rm inj} = 0.59$, QCLs exhibit QP state with the period of $1/f_\Delta$. In the time range of one period, higher-frequency oscillation can be observed. In the power spectra, apart from the peaks at integer multiples of f_Δ, there are also some peaks at the frequencies higher than 40 GHz. In the optical spectrum, narrow peaks can be observed.

3.4. Mapping of dynamic states

In order to furtherly understand the dynamic behaviors in QCLs, the mapping of dynamic states in the parameter space of Δf and $k_{\rm inj}$ is presented in Fig. 9(a). In the figure, different dynamic states are shown by different colors. The blue zones represent the P1 state. Two P1 zones can be observed: the lower left one is the P1 resulted from the external-cavity periodic dynamic, the lower right one is the P1 resulted from optical modes beating. The light-blue zone represents the SW state. The SW state zone is only observed in the range of detuning frequency lower than 10 GHz, where complete injection locking can be achieved. The green zone represents the QP state. The QP state zone actually consists of three parts: external-cavity QP state zone (examples in Figs. 4(c) and 5(d)), optical modes beating QP state zone (example in Fig. 8(c)), and the bioscillation QP state zone (examples in Figs. 6(b) and 7(b)). The light-green zones represent the PB state. The PB state zones are multiple discrete small zones, which are distributed in the QP state zone, where strong interaction of the external-cavity periodic dynamic and the optical modes beating periodic dynamic occurs. The white zone represents the chaotic (C) state.

Figure 9(b) shows the chaos bandwidth in the parameter space, which is given by the red dash line box in Fig. 9(a). Two types of chaotic states are given the names of chaos and chaos(Δf), which are distinguished by whether there is a wide envelope peak at Δf. The black dash line is the boundary between chaos and chaos(Δf). In the chaos zone, the bandwidth is always around 14 GHz. In the chaos(Δf) zone, the bandwidth increases gradually with the increase of Δf, showing the way to generate mid-infrared wide-band chaotic laser in mutual-coupled QCLs.

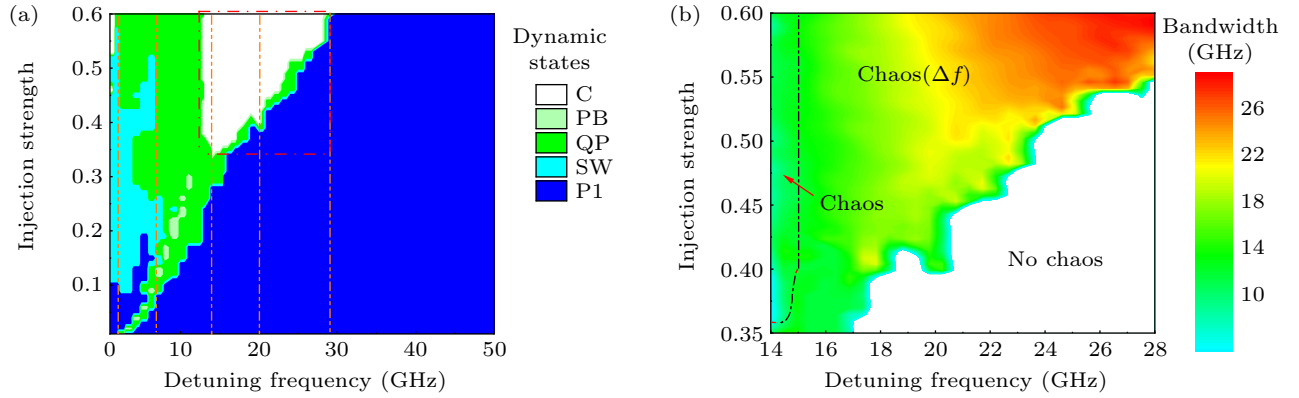


Fig. 9. (a) Mapping of dynamical states in the parameter space of detuning frequency Δf and injection strength $k_{\rm inj}$. P1: period-one; SW: square wave; QP: quasi period; PB: pulse burst; C: chaos. The orange dashed line from left to right represents the detuning frequencies of 2 GHz, 7 GHz, 14 GHz, 20 GHz, and 29 GHz respectively. (b) Bandwidth of chaotic state in parameter space of Δf and $k_{\rm inj}$, given by the red dash line box in (a).

4. Conclusion

We numerically investigated the dynamic states in mutual-coupled mid-infrared QCLs and discussed the physical mechanism of dynamic states evolution. Three types of P1 states with different periods were found, which were $\tau_{\rm inj}$, $2\tau_{\rm inj}$, and reciprocal of the detuning frequency. There was no relaxation oscillation observed. By changing the injection strength and detuning frequency, several other dynamic states were demonstrated, including SW, QP, PB, and chaotic laser. The external-cavity periodic dynamics and optical modes beating are the mainly periodic dynamics. High-order harmonics dynamics and strong optical nonlinear can be stimulated by strong injection. When Δf is small or very large, the interaction of the two periodic dynamics is very weak. Strong injection can drive the P1 state to SW and QP states. When Δf is in the proper range, strong interaction of the two periodic dynamics occurs, leading to PB state and chaotic state. The PB state can be thought as an intermittent chaotic state. Strong injection can make the chaotic state more stable. This work helps to understand the physics mechanism of dynamic behaviors in QCLs and open a new way to mid-infrared wide-band chaotic laser.

Acknowledgments

Project supported by the National Key Research and Development Program of China (Grant No. 2019YFB1803500), the National Natural Science Foundation of China (Grant No. 61805168), the Natural Science Foundation of Shanxi Province, China (Grant Nos. 201801D221183 and 20210302123185), International Cooperation of Key Research and Development Program of Shanxi Province (Grant No. 201903D421012), Research Project Supported by Shanxi Scholarship Council of China (Grant No. 2021-032), Scientific and Technological Innovation Programs of Higher Education Institutions in Shanxi (Grant No. 2019L0133), and Fund for Shanxi "1331 Project" Key Innovative Research Team.

References

[1] Faist J, Capasso F, Sivco D L, Sirtori C, Hutchinson A L and Cho A Y 1994 *Science* **264** 553
[2] Liu Y H, Zhang J C, Yan F L, Jia Z W, Liu F Q, Liang P, Zhuo N, Zhai S Q, Wang L J, Liu J Q, Liu S M and Wang Z G 2016 *Opt. Exp.* **24** 19545
[3] Vitiello M S, Scalari G, Williams B and Natale P De 2015 *Opt. Exp.* **23** 5167
[4] Wang H, Zhang J C, Cheng F M, Zhuo N, Zhai S Q, Liu J Q, Wang L J, Liu S M, Liu F Q and Wang Z G 2020 *Opt. Exp.* **28** 40155
[5] Fei T, Zhai S Q, Zhang J C, Zhuo N, Liu J Q, Wang L J, Liu S M, Jia Z W, Li K and Sun Y Q 2021 *J. Semicond.* **42** 112301
[6] Liu C W, Zhai S Q, Zhang J C, Zhou Y H, Jia Z W, Liu F Q and Wang Z G 2015 *J. Semicond.* **36** 094009
[7] Spitz O, Didier P, Durupt L, Díaz-Thomas D A, Baranov A N, Cerutti L and Grillot F 2021 *J. Select. Topics Quantum Electron* **28** 1200109
[8] Pang X D, Ozolins O, Schatz R, Storck J, Udalcovs A, Navarro J R, Kakkar A, Maisons G, Carras M and Jacobsen G 2017 *Opt. Lett.* **42** 3646
[9] Paschke K, Liu P Q, Michel A P, Smith J, Moshary F and Gmachl C 2010 *Conference on Lasers and Electro-Optics*, May 16–21, 2010, San Jose, California United States, p. JThJ3
[10] Gregorio E and Rocadenbosch F 2007 *IEEE International Geoscience and Remote Sensing Symposium (IGARSS)*, July 23–27, 2007, Barcelona, Spain, p. 2955
[11] Chien H T, Wang K, Sheen S H and Raptis A C P 2012 *Conference on Chemical, Biological, Radiological, Nuclear and Explosives (CBRNE) Sensing XIII*, April 24–27, 2012, Baltimore, Maryland, p. 83581K
[12] Abramov P I, Kuznetsov E V and Skvortsov L A 2017 *J. Opt. Technol.* **84** 331
[13] Langley L N, Turovets S and Shore K A 1995 *Opt. Lett.* **20** 725
[14] Eriksson S and Lindberg Å M 2001 *Opt. Lett.* **26** 142
[15] Sciamanna M and Shore K A 2015 *Nat. Photonics* **9** 151
[16] Soriano M C, García-Ojalvo J, Mirasso C R and Fischer I 2013 *Rev. Mod. Phys.* **85** 421
[17] Mork J, Tromborg B and Christiansen P L 1988 *IEEE J Quantum Electron* **24** 123
[18] Yamasaki K, Kanno K, Matsumoto A, Akahane K, Yamamoto N, Naruse M and Uchida A 2021 *Opt. Exp.* **29** 17962
[19] Azouigui S, Kelleher B, Hegarty S P, Huyet G, Dagens B, Lelarge F, Accard A, Make D, Le Gouezigou O and Merghem K 2007 *Opt. Exp.* **15** 14155
[20] Heil T, Fischer I, Elsäßer W and Gavrielides A 2001 *Phys. Rev. Lett.* **87** 243901
[21] Liu S, Lalanne E, Kuis R and Johnson A 2009 *Frontiers in Optics*, October 11–15, 2009, San Jose, California United States, p. PDPA3
[22] Jumpertz L, Michel F, Pawlus R, Elsässer W, Schires K, Carras M and Grillot F 2016 *AIP Adv.* **6** 015212
[23] Mezzapesa F P, Columbo L L, Brambilla M, Dabbicco M, Borri S, Vitiello M S, Beere H E, Ritchie D A and Scamarcio G 2013 *Opt. Exp.* **21** 13748
[24] Jumpertz L, Schires K, Carras M, Sciamanna M and Grillot F 2016 *Light Sci. Appl.* **5** e16088

[25] Wang X G, Zhao B B, Deng Y, Kovanis V and Wang C 2021 *Phys Rev A.* **103** 023528
[26] Zhao B B, Wang X G and Wang C 2022 *J. Select. Topics Quantum Electron* **28** 1800207
[27] Zhao B B, Kovanis V and Wang C 2019 *J. Select. Topics Quantum Electron* **25** 1900207
[28] Vukovic N N, Radovanovic J V, Milanovic V B, Antonov A V, Kuritsyn D I, Vaks V V and Boiko D L 2019 arXiv: 1902.00205
[29] Chen C J, Jia Z W, Lv Y X, Li P, Xu B J and Wang Y C 2021 *Opt. Lett.* **46** 5039
[30] Paiella R, Martini R, Capasso F, Gmachl C, Hwang H Y, Sivco D L, Baillargeon J N, Cho A Y, Whittaker E A and Liu H C 2001 *Appl. Phys. Lett.* **79** 2526
[31] Kuwashima F and Iwasawa H 2007 *Jpn. J. Appl. Phys.* **46** 1526
[32] Zhang T, Jia Z W, Wang A B, Hong Y H, Wang L S, Guo Y Y and Wang Y C 2021 *IEEE Photon. Technol. Lett.* **33** 335